Synthesis of hexagonal Ni_3N using high pressures and temperatures

2006 J. Phys.: Condens. Matter 18 8651

(http://iopscience.iop.org/0953-8984/18/37/021)

INSTITUTE OF PHYSICS PUBLISHING JOURNAL OF PHYSICS: CONDENSED MATTER

J. Phys.: Condens. Matter **18** (2006) 8651–8660 doi:10.1088/0953-8984/18/37/021

Synthesis of hexagonal Ni_3N using high pressures and temperatures

C Guillaume[1], J P Morniroli[2], D J Frost[3] and G Serghiou[1]

[1] University of Edinburgh, School of Engineering and Electronics and Centre for Materials Science, Kings Buildings, Mayfield Road, EH9 3JL, UK
[2] Laboratoire de Metallurgie Physique et Genie des Materiaux, UMR CNRS 8517, Universite des Sciences et Technologies de Lille et Ecole Nationale Superieure de Chimie de Lille, Cite Scientifique, 59655 Villeneuve d'Ascq Cedex, France
[3] Bayerisches Geoinstitut, Universitat Bayreuth, D-95440, Bayreuth, Germany

E-mail: george.serghiou@ed.ac.uk

Received 27 April 2006, in final form 21 July 2006
Published 1 September 2006
Online at stacks.iop.org/JPhysCM/18/8651

Abstract

The only known bulk ambient pressure nickel nitride phase is hexagonal Ni_3N (space group $P6_322$). Multianvil synthesis experiments at 20 GPa and 2000 K using nickel (Ni) and sodium azide (NaN_3) starting materials, and *ex situ* analysis using transmission electron microscopy and scanning electron microscopy measurements show that this phase can be recovered at ambient pressure (space group $P6_322$, $a = 4.62$ Å, $c = 4.30$ Å, $Z = 2$). Formation of this phase is correlated with the repulsive interactions between closely spaced nitrogen ions and with the extent of thermal stability of nickel nitride at ambient and at high densities. These two factors are also important in relating the high temperature and pressure behaviour of nickel nitride to those of several other interstitial nitrides recovered from similar pressures after heating. Further, we report formation of a sodium rhenium nitride phase by reaction of the azide with the rhenium capsule in which the reactants were contained.

1. Introduction

Nitrides are emerging as a class of materials having technological and crystal chemical importance [1]. Despite this fact, and the almost three to one relative atmospheric atomic abundance of nitrogen to oxygen, synthesized or naturally occurring oxides exceed nitrides by at least two orders of magnitude. For synthetic systems, this difference is in part due to the greater difficulties in processing pure nitrides. For high density systems in particular, the preponderance of oxide data also stems from the long-standing interest in understanding the oxide-based structure and properties of our planet's interior [2]. These efforts have contributed considerably to the charting of the high density oxide landscape, particularly via studies on

silicate based oxides where increases in density are typically accommodated by an increase in oxygen coordination around silicon from four to six [3]. The principal results in the nascent high density nitride landscape so far have included new crystal classes (cubic spinel) of binary group IVA nitrides (Si, Ge, Sn) [4–6] (high density carbon nitride has not been verified), to novel thorium phosphide structured binary group IVB (Zr, Hf) nitrides (titanium (Ti) nitride retains its ambient pressure rocksalt structure) [7]. Moreover, a cubic platinum nitride has been reported [8], as well as ordered hexagonal molybdenum nitride [9]. Further, the well known superhard cubic boron nitride is also prepared at high pressure [10, 11] and GaN, while retaining its ambient condition wurtzite structure, can, at pressure, be prepared as a dislocation-free single crystal [12].

Thus we observe a diversity of behaviours even within the same groups in this nascent nitride landscape at high densities, ranging from new structural forms (e.g. Si, Ge, Sn, Hf, Zr)–N [4–7] to noteworthy stability of the ambient pressure form (e.g. TiN) or no stability at all (e.g. C–N) [13]. Here we probe the nitride landscape by investigating the stability of nickel nitride at high pressures and temperatures. Nickel nitride belongs to the broader class of interstitial nitrides which includes ambient pressure (Hf, Zr, Ti)–N forms [14–16]. Interstitial nitrides are generally characterized by a host metal which differs markedly in terms of electronegativity and atomic size from nitrogen. The nitrogen is situated in interstitial octahedral sites within the host metal whose structure changes to accommodate the nitrogen [15]. Unlike the early (IVB) (Hf, Zr, Ti)–N interstitial nitrides which are highly refractory with melting points above 3000 K, later (VIIIB) interstitial nitrides in the order (Fe–Co–Ni)–N decompose below about 1000 K at ambient pressure [17]. Nickel nitride in particular decomposes to nickel and molecular nitrogen, starting at about 600 K. The decreasing stability of the later nitrides is also reflected by the increasing difficulty in their ambient pressure preparation. While group IV–VI nitrides can be prepared by nitriding the metal in molecular nitrogen, bulk (Fe–Co–Ni)–N nitrides require ammonia (NH_3), that is, nitrogen, essentially, in atomic form [16]. Nickel nitrides in particular have typically been prepared in bulk syntheses by heating nickel powder or nickel halide and alkali amides in a flowing stream of ammonia at temperatures of between 500 and 700 K, well below the 1730 K melting point of nickel [15–21]. Nickel nitride preparations have also been reported through reactive sputtering of nickel films in Ar/N_2 gas mixtures, as well as through ion bombardment of nickel films using N^+ ions [22–28]. The bulk syntheses have invariably given rise to the Ni_3N stoichiometry with hexagonal symmetry and a $P6_322$ space group [17, 19]. In this arrangement one third of the octahedral voids present in the hexagonal close packing of nickel atoms are occupied by nitrogen. The NNi_6 octahedra share common vertices only, and the nitrogen atoms in most of these syntheses have shown essentially complete occupational order [17, 19]. The sputtering and ion implantation methods have also given rise to this hexagonal structure with nitrogen exhibiting both ordered as well as disordered arrangements depending on the particular experimental conditions [22, 25, 27, 28]. Other structures and stoichiometries reported using these latter methods include cubic Ni_8N [22], cubic as well as tetragonal modifications of Ni_4N [26] and a tetragonal Ni_2N modification [23, 24].

In this study we investigate the effect of high pressure and temperature on the synthesis of nickel nitride using nickel and sodium azide starting materials, with the latter serving as a nitrogen provider for nitride synthesis in a multianvil apparatus. We employ scanning electron microscopy as well as transmission electron microscopy for chemical, morphological and structural characterization of the reaction products. Together with the development of correlations for the high density behaviour of interstitial nitrides we also demonstrate metal to metal nitride synthesis in a large volume press under very extreme conditions.

2. Experimental techniques

The starting materials for the synthesis were nickel (99.7%) and sodium azide (99.99+%) powders (Aldrich). An approximate mixture of 30 at.% nickel (Ni) and 70 at.% sodium azide (NaN_3) was loaded into a capsule made of 0.025 μm thick rhenium foil. The capsule was made by double-wrapping the rhenium foil around a 1.4 mm post. Before crimping the rhenium foil shut on both sides, three rhenium discs were added to the bottom side. The mixture was then placed on top of these discs, and then two further discs were placed on top of the mixture to further seal the capsule against loss of potential fluid reactants and products. These top discs were then gently tapped to decrease the void space in the capsule. The final packed capsule size was 1.6 mm wide and 1.8 mm long. These dimensions are needed to adjust the further element sizes inside the furnace (see below). The capsule was then placed in a desiccator until its placement in the final high pressure assembly. High pressures and temperatures of 20 GPa and 2000 K were applied using a multianvil apparatus (Hymag, 1000 ton hydraulic press) and a $LaCrO_3$ heater, respectively, at the Bayerisches Geoinstitut [29, 30]. The pressure assembly consisted of Cr-doped MgO octahedra with a 10 mm edge length which were compressed by eight tungsten carbide cubes (32 mm edge) with 5 mm truncation edge lengths. This configuration constitutes a 10/5 assembly. Before loading the capsule, the MgO octahedra, an insulating ZrO_2 sleeve, the $LaCrO_3$ furnace and the MgO and crushable Al_2O_3 spacers were first fired at 1300 K for 1 h to eliminate any traces of water. Then these elements were mounted together without the capsule. A molybdenum ring was also inserted to provide electrical contact between the $LaCrO_3$ furnace and the WC anvils. A $W_{97}Re_3/W_{75}Re_{25}$ thermocouple was next incorporated for the temperature measurement. The thermocouple wires were placed in an alumina insulating sleeve in order to allow the two wires to cross each other only where the temperature is to be read, that is, at the top of the rhenium capsule. Ceramic cement was used in order to keep the thermocouples in place and to fill the remaining void spaces in the assembly. This assembly, still without the capsule, was dried overnight on top of an oven. Once the pressure assembly was dried, the capsule was placed in the middle of the MgO octahedra. A molybdenum disc was then used to close the other MgO octahedral entrance and simultaneously provide electrical contact with the other end of the $LaCrO_3$ furnace and the power supply. The eight anvils which are used to apply the pressure were prepared next. First, pyrophyllite gaskets were glued around the truncations of four of the anvils. Then cardboard paper was glued on the three faces where pyrophyllite was placed, for electrical insulation. Further electrical insulation was provided by covering the three faces adjacent to the truncations of the other four anvils with some insulating tape. The pressure assembly was then placed at the centre of the eight anvils. Finally, glass fibre reinforced epoxy foils were glued on the six faces of the eight-anvil cluster to secure the pressure assembly in position while placing the cluster in the press. Before placing the cluster in the press, two copper sheets (electrical contacts) were added to two of the glass fibre foils to allow the current to pass through the two cubes which touch the molybdenum disc and ring, respectively, while pressure is applied. This set-up was then positioned in the multianvil and the thermocouple connections established. Pressure was applied hydraulically. The target pressure of 20 GPa was reached after 4 h. The target temperature of 2000 K was attained in 20 min. The sample was held at this temperature for 1 min, and then cooled to room temperature in about 20 min. The pressure was then released over a period of 17 h in order to minimize damage to the carbide anvils. The pressure assembly was then dismantled to retrieve the capsule.

The rhenium capsule was then cut along the vertical axis, with an annular 170 μm wide diamond blade. Oil instead of a more conventional water-based lubricant was used to protect against any potential hygroscopic effects. One half of the capsule was mounted in epoxy resin

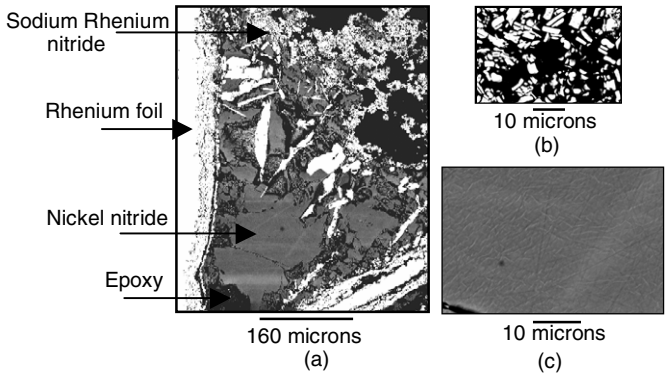

Figure 1. Backscattered scanning electron microscopy (BSE) image of a section of one half of the recovered cylindrical rhenium capsule from 20 GPa and 2000 K, after it was cut using a diamond saw. There are three distinct regions, as labelled in the figure, and the epoxy in which the capsule is embedded for SEM measurements (a). Higher magnification BSE images of the sodium rhenium nitride (b) and nickel nitride reaction products (c).

and dried overnight. The epoxy resin block was ground for a few minutes with a 5 μm diamond sheet (Buehler Ultraprep), in order to reach the surface of the sample. Then, the sample surface was polished with 3 μm diamond paste (Kemet) together with a lapping oil lubricant (Buehler Automet) on a standard polishing cloth (Kemet PSU-M) for about 15 min. Finally, the sample was further polished with the same polishing cloth for about 10 min using 1 μm diamond paste (DP Suspension, Struers).

The sample was then carbon coated for scanning electron microscopy (Philips XL30CP, with an energy dispersive x-ray analyser (Oxford Instruments EDX detector—SiLi crystal with PGT Spirit Analysis software) for chemical analysis. The acceleration voltages used were 10 and 20 kV in backscattering electron mode for chemical contrast. The lower voltage served to enhance detection of the nitrogen light element by reducing the effect of x-ray absorption [31]. The sample was also investigated with a Philips CM30 transmission electron microscope (TEM), equipped with a Gatan SS CCD camera and with Digital Micrograph software for the acquisition of electron diffraction patterns and bright-field imaging. Particles of the reaction product from the polished half capsule were taken under an 126× total magnification optical microscope, using a sharp tungsten carbide needle and dispersed onto the thin carbon film of a labelled 3 mm diameter copper grid (Agar Scientific). Electron diffraction and bright-field images were obtained using 300 kV acceleration voltage. A 440 mm camera length was used for recording electron diffraction patterns. Both selected-area electron diffraction (SAED) and microdiffraction (electron diffraction with a nearly parallel incident beam focused on the specimen with a small spotsize in the range 10–50 nm) were used for collecting diffraction patterns [32–34]. SAED was used for collecting ring patterns from the polycrystalline matrix. Microdiffraction was used for obtaining zone-axis diffraction spot patterns from individual grains.

3. Results and discussion

The sample recovered from 20 GPa and 2000 K exhibits three distinct chemistries (figure 1(a)). The first is the rhenium capsule as also verified by EDX measurements (figure 2(a)). The second consists of brick shaped grains belonging to a sodium rhenium nitride phase obtained

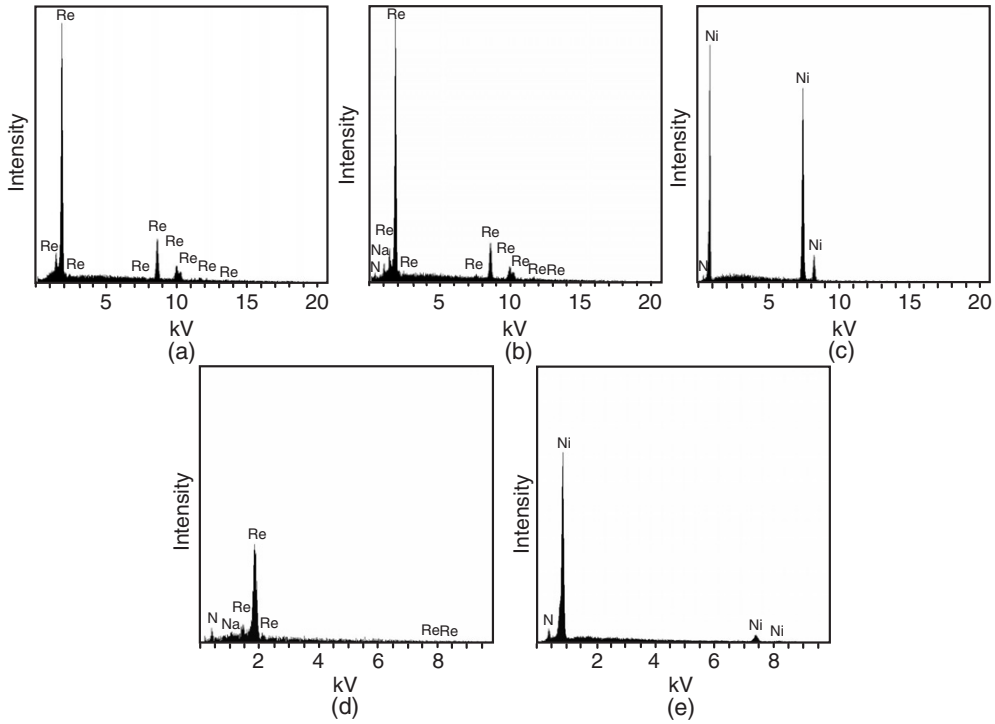

Figure 2. Energy dispersive x-ray analysis (EDX) spectra of the rhenium foil (a), the sodium rhenium nitride reaction product (b, d), and the nickel nitride reaction product (c, e). We have observed formation of the sodium rhenium nitride phase in several syntheses employing sodium azide and metal starting materials encapsulated in a rhenium foil, for example copper and sodium azide to 20 GPa and 2000 K which results in pure copper and sodium rhenium nitride. Further high pressure and temperature metal nitride reactions with rhenium have also been documented and will be the focus of further studies [13].

from reaction of the azide with the foil (figure 1(b)). The EDX spectrum shown in figure 2(b) was representative of all the brick shaped grains examined. The structure and chemistry of this ternary phase will be the focus of a further study. The third region, and the focus of this work, is nickel nitride, with spectra from numerous spots all showing virtually the same intensity ratios as in figure 2(c) using 20 kV excitation voltage. The relative intensity of the nitrogen peaks was enhanced by using 10 kV excitation as well (figures 2(d), (e)). The morphology and texture of the nickel nitride appears uniform based on scanning electron microscopy images (figure 1(c)).

Higher magnification images of nickel nitride taken with the transmission electron microscope reveal the presence of numerous crystallites (figure 3).

To investigate the structure of the individual crystallites, whose sizes ranged from about 20 to 50 nm, microdiffraction was employed [32]. Zone axis diffraction patterns were collected from several crystals, two of which were taken along [0001] and $[\bar{1}013]$ as shown in figures 4(a) and (b). All the zone axis diffraction patterns collected were interpreted using the program Electron Diffraction version 7.01 [35] and showed a good fit to the ordered hexagonal Ni_3N structure with space group $P6_322$ and lattice parameters $a = 4.622$ Å, $c = 4.306$ Å, $Z = 2$. Several ring patterns were also recorded using SAED. These range markedly in texture, exhibiting spotty to smooth as well as sharp to broadened rings (figures 5(a), (b)). The observed rings, matched rings belonging to the ordered hexagonal Ni_3N phase.

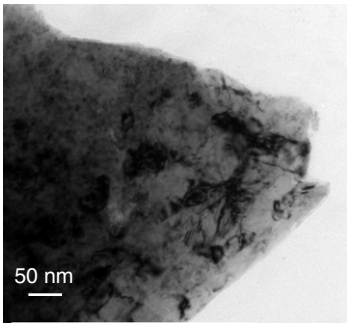

Figure 3. Bright field transmission electron microscope image of a section of the nickel nitride sample placed inside a carbon grid.

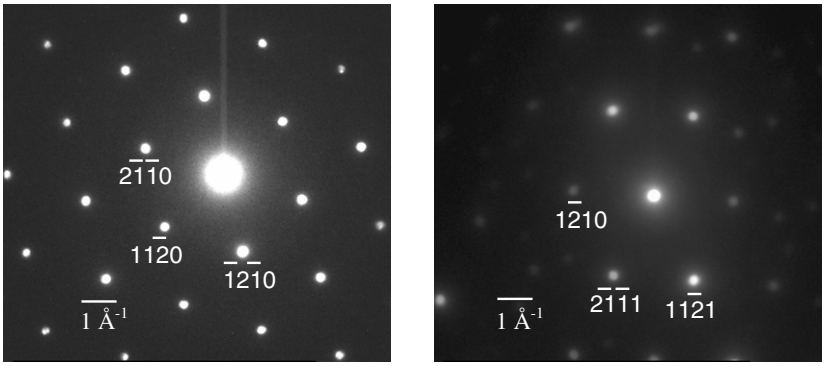

Figure 4. Microdiffraction zone-axis diffraction spot patterns of zones [0001] (a) and [$\bar{1}$013] (b) of the hexagonal (S.G. $P6_322$) nickel nitride (Ni_3N) structure.

Thus, based on these measurements, hexagonal Ni_3N is recovered after compression at 20 GPa and heating at 2000 K. Hexagonal nickel nitride is also the only nickel nitride modification that can be prepared in the bulk at ambient pressure [17]. The results are, on the one hand, similar to those of TiN which retains its ambient pressure structure after heating at 18 GPa to 3000 K, but are different from those of the other two early interstitial nitrides, namely zirconium and hafnium nitride which form new cubic dense nitrides with A_3N_4 stoichiometry under those conditions as well as lower pressures to at least 15 GPa. The new phases are recovered to ambient pressure [7]. A pressure of 100 GPa and 2800 K were proposed to make Ti_3N_4 thermodynamically favourable with respect to TiN and N_2 [36, 37], or even higher unspecified temperatures to promote removal of an electron from Ti and thus facilitate the higher 3:4 stoichiometry [38].

We identify here two factors which, consistent with the experimental observations, act against nickel nitride and titanium nitride forming denser phases at high pressures and temperatures and which correlate with the formation of denser A_3N_4 structures for the Zr and Hf interstitial nitrides. These factors are: short nitrogen distances and the degree of thermal stability. We discuss N–N distances first. The cubic $(Hf, Zr)_3N_4$ modifications (lattice constants of about $a = 6.7$ Å), have tightly packed $N(Hf, Zr)_6$ polyhedral units which share faces along the body diagonals of the cubic cell, and have shortest N–N distances of about 2.7 Å along the face-sharing directions [39, 40]. This short distance leads, according to models

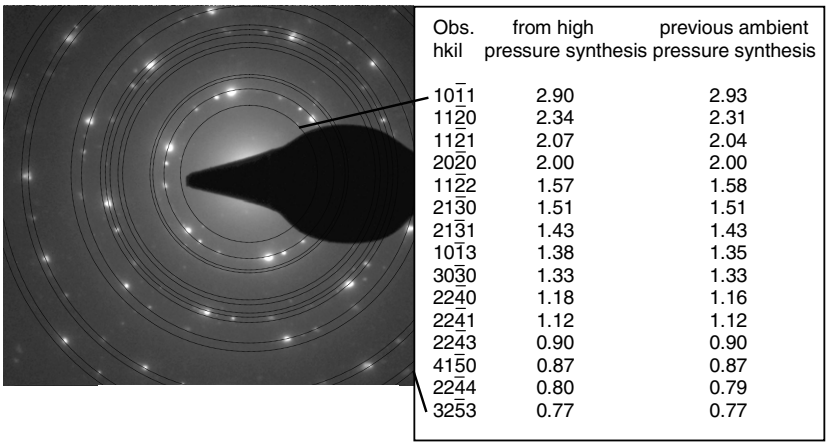

Obs. hkil	from high pressure synthesis	previous ambient pressure synthesis
$10\bar{1}1$	2.90	2.93
$11\bar{2}0$	2.34	2.31
$11\bar{2}1$	2.07	2.04
$20\bar{2}0$	2.00	2.00
$11\bar{2}2$	1.57	1.58
$21\bar{3}0$	1.51	1.51
$21\bar{3}1$	1.43	1.43
$10\bar{1}3$	1.38	1.35
$30\bar{3}0$	1.33	1.33
$22\bar{4}0$	1.18	1.16
$22\bar{4}1$	1.12	1.12
$22\bar{4}3$	0.90	0.90
$41\bar{5}0$	0.87	0.87
$22\bar{4}4$	0.80	0.79
$32\bar{5}3$	0.77	0.77

(a)

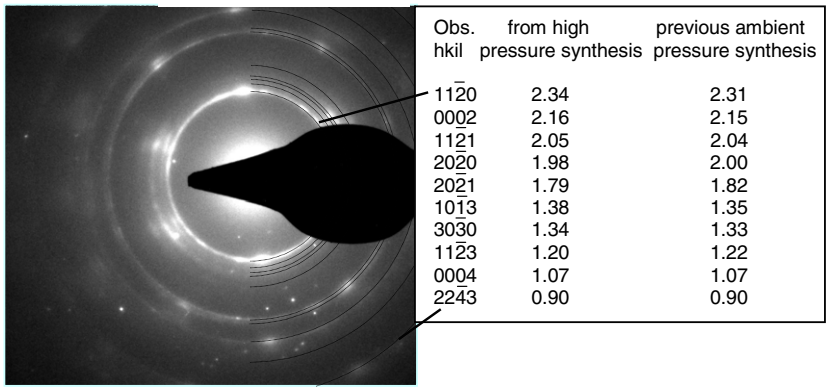

Obs. hkil	from high pressure synthesis	previous ambient pressure synthesis
$11\bar{2}0$	2.34	2.31
$000\bar{2}$	2.16	2.15
$11\bar{2}1$	2.05	2.04
$20\bar{2}0$	1.98	2.00
$20\bar{2}1$	1.79	1.82
$10\bar{1}3$	1.38	1.35
$30\bar{3}0$	1.34	1.33
$11\bar{2}3$	1.20	1.22
$000\bar{4}$	1.07	1.07
$22\bar{4}3$	0.90	0.90

(b)

Figure 5. Selected area electron diffraction (SAED) ring patterns taken from the nickel nitride sample. The patterns range from spotty to smooth and sharp to diffuse (a), (b). Full trace circles are used for clarity in the spotty ring pattern (a). Lattice spacings of the recovered nickel nitride match rings of hexagonal nickel nitride (space group $P6_322$ and lattice parameters $a = 4.622$ Å, $c = 4.306$ Å, $Z = 2$) prepared at ambient conditions.

of pair potentials in interstitial compounds, to enhanced repulsive interactions between nitrogen ions in such systems [41–43]. Based on first principles simulations, the lattice constant and shortest N–N distance in cubic Ti_3N_4 would be about 2.5 Å [36]. This is likely to lead to even more pronounced strain interactions in this system, resulting in the rocksalt TiN persisting as the favourable modification at high pressure. These structural considerations carry over to the late interstitial nitrides, and nickel nitride in particular [17, 44]. In proceeding from ordered hexagonal Fe_3N to ordered hexagonal Ni_3N there is a significant contraction in unit cell parameters, from $a = 4.694$ to 4.622 Å, and $c = 4.375$ to 4.306 Å, respectively. This is reflected by a shortening of the N–N interatomic distances from 3.5 Å down to 3.42 Å which, in turn, leads to enhanced repulsive interactions between nitrogen ions located in the centres of adjacent octahedra [17]. These repulsive interactions are minimized when the nitrogens are furthest apart. This is the case when the nitrogen octahedra only share common corners. Indeed the hexagonal AN_x stoichiometry ($x = 1/3$) having an ordered distribution of nitrogens filling one third of the octahedral positions, only has corner connected octahedra, thus minimizing

the strain induced interactions. Deviation from this stoichiometry and ordered arrangement requires edge sharing, and for even higher nitrogen contents, face sharing octahedra as well, leading to shorter N–N distances [17]. This would cause the largest strains to the nickel nitride lattice with its inherently shortest N–N distances amongst the late interstitial nitrides. Indeed, this has been put forward to explain why, in contrast to the other interstitial nitrides with hexagonal symmetry, nickel nitride (NiN_x) is constrained to the $x = 1/3$ stoichiometry. Contrastingly the other interstitial nitrides with their larger lattice constants, such as iron and manganese, can be formed in a number of non-stoichiometric configurations ($x > 1/3$) containing edge [44] and even face sharing [45] nitrogen centred octahedra. Application of pressure will require a closer packed arrangement of ions, and in particular the adoption of shorter N–N distances to which nickel nitride is particularly resistant, even at ambient pressure. Moreover, the overall trend in nitride syntheses, that nitrogen to cation stoichiometric ratios increase with higher nitrogen pressures [46], would probably be difficult to accommodate in an ordered arrangement. This is again because in MN_x, (M = Mn, Fe, Co, Ni) as x increases much above $1/3$, which is the ideal for perfect order, more and more interstitial sites must be filled in other Wyckoff sites beyond 2c, leading to increased edge sharing and thus unfavourable closer N–N distances. This is particularly unfavourable for NiN_x with its smaller lattice constants.

In the early (Zr, Hf)–N interstitial nitrides, kinetic barriers for transition to close packed configurations could be overcome by high temperatures, and indeed temperatures to 3000 K have been employed [7]. This is a feasible synthetic route for these early interstitial nitrides since they have high melting points exceeding 3000 K even at ambient pressure [15]. The late interstitial nitrides (Fe, Co, Ni)–N, contrastingly, do not melt but dissociate above about 600 K [14, 16]. Indeed high melting points have been correlated with high cation–nitrogen bond energies and high heats of formation [15]. The heats of formation of the early interstitial nitrides are more than an order of magnitude higher than those of the late interstitial nitrides [47, 48]. Therefore, for late interstitial nitrides, overcoming kinetic and possibly ionization energy barriers at high temperatures competes with their tendency to dissociate. Thus, although pressure generally expands the temperature stability field of a metal nitride with respect to the free metal and N_2 [12], formation of a denser nickel nitride is less facile than for early interstitial nitrides which have melting points about five times higher than late interstitial nitride dissociation temperatures.

4. Conclusions

In this work we have recovered hexagonal nickel nitride after heating elemental nickel and sodium azide at 2000 K and 20 GPa in a multianvil apparatus. This temperature is more than three times its dissociation temperature at ambient pressure, and only 100 K below the melting point of nickel at 20 GPa [49]. We have identified the shortest nitrogen interatomic distances and the degree of thermal stability as important factors influencing whether denser phases will form in both early and late interstitial nitrides. This therefore constitutes a novel and significant step in charting the emerging landscape. Diamond cell experiments employing N_2 heated with metal or metal nitride substrates will also further our knowledge of this important materials domain.

Acknowledgments

High pressure experiments were performed at the Bayerisches Geoinstitut under the EU 'Research Infrastructures: Transnational Access' Programme (contract no 505320 (RITA)—

High Pressure). We also acknowledge the use of the EPSRC Chemical Database Service at Daresbury and the particularly generous assistance of R A Meeking. We further thank, N Odling for many discussions, J Craven for assistance with scanning microscopy, M Hall for demanding solids processing, L Nigay for a critical reading of the manuscript as well as A Buts and M Mijajlovic for further assistance.

References

[1] Lowther J E, Amkreutz M, Frauenheim T, Kroke E and Riedel R 2003 *Phys. Rev.* B **68** 033201
[2] Ringwood A E 1996 *Phys. Earth Planet. Inter.* **86** 79
[3] Serghiou G, Boehler R and Chopelas A 2000 *J. Phys.: Condens. Matter* **12** 849
[4] Zerr A, Miehe G, Serghiou G, Schwarz M, Kroke E, Riedel R, Fuess H, Kroll P and Boehler R 1999 *Nature* **400** 340
[5] Serghiou G, Miehe G, Tschauner O, Zerr A and Boehler R 1999 *J. Chem. Phys.* **111** 4659
[6] Scotti N, Kockelmann W, Senker J, Trassel S and Jacobs H 1999 *Z. Anorg. Allg. Chem.* **625** 1435
[7] Zerr A, Miehe G and Riedel R 2003 *Nat. Mater.* **2** 185
[8] Gregoryanz E, Sanloup C, Somayazulu M, Badro J, Fiquet G, Mao H K and Hemley R J 2004 *Nat. Mater.* **3** 294
[9] Bull C L, McMillan P F, Soignard E and Leinenweber K 2004 *J. Solid State Chem.* **177** 1488
[10] Wentorf R H 1957 *J. Chem. Phys.* **26** 956
[11] Solozhenko V L, Turkevich V Z and Holzapfel W B 1999 *J. Phys. Chem.* B **103** 2903
[12] Grzegory I 2002 *J. Phys.: Condens. Matter* **14** 11055
[13] Serghiou G 2006 in preparation
[14] Wells A F 1986 *Structural Inorganic Chemistry* (Oxford: Clarendon)
[15] Pierson H O 1996 *Handbook of Refractory Carbides and Nitrides: Properties, Characteristics, Processing and Applications* (New Jersey: Noyes)
[16] Goldschmidt H J 1967 *Interstitial Alloys* (London: Butterworths)
[17] Leineweber A, Jacobs H and Hull S 2001 *Inorg. Chem.* **40** 5818
[18] Juza R and Sachsze W 1943 *Z. Anorg. Allg. Chem.* **251** 201
[19] Leinenweber A, Jacobs H, Kockelmann W, Hull S and Hinz-Hubner D 2004 *J. Alloys Compounds* **384** 1
[20] Massalski T 1990 *Binary Alloy Phase Diagrams* (Ohio: ASM)
[21] Desmounis-Krawiec S, Aymonier C, Loppinet-Serani A, Weill F, Gorsse S, Etourneau J and Cansell F 2004 *J. Chem. Mater.* **14** 228
[22] Neklyudov I M and Morozov A N 2004 *Physica* B **350** 325
[23] Dorman G J W R and Sikkens M 1983 *Thin Solid Films* **105** 251
[24] Kawamura M, Abe Y and Sasaki K 2000 *Vacuum* **59** 721
[25] Auguin B, Vigner D and Riwan R 1967 *C. R. Acad. Sci.* **264** 809
[26] Terao P N 1960 *J. Phys. Soc. Japan* **15** 227
[27] Bykov V N, Troyan V A, Zdorovtseva G G and Khaimovich V S 1975 *Phys. Status Solidi* a **32** 53
[28] Terao P N and Berghezan A 1959 *J. Phys. Soc. Japan* **14** 139
[29] Frost D J, Poe B T, Tronnes R G, Liebske C, Duba A and Rubie D C 2004 *Phys. Earth Planet. Inter.* **143** 507
[30] Rubie D C 1999 *Phase Transit.* **68** 431
[31] Goldstein J I, Newbury D E, Patrick E, Joy D C, Romig A D, Lyman C E, Fioru C and Lifshin E 1992 *Scanning Electron Microscopy and X-ray Microanalysis* (New York: Plenum)
[32] Morniroli J P, No M L, Rodriguez P P, San Juan J, Jezierska E, Michel N, Poulat S and Priester L 2003 *Ultramicroscopy* **98** 9
[33] Holmestad R, Morniroli J P, Zuo J M, Spence J C H and Avilov A 1997 *Electron Microsc.* **153** 137
[34] Williams D B and Barry Carter C 1996 *Transmission Electron Microscopy* (New York: Plenum)
[35] Morniroli J P 2004 *ENS Lille UMR CNRS 8517, France*
[36] Kroll P 2003 *Phys. Rev. Lett.* **90** 125501
[37] Kroll P 2004 *J. Phys.: Condens. Matter* **16** 1235
[38] Li X J, Kobayashi T C and Sekine T 2004 *Solid State Commun.* **130** 79
[39] O'Keefe M and Andersson S 1977 *Acta Crystallogr.* A **33** 914
[40] Fletcher D A, McMeeking R F and Parkin D 1996 *J. Chem. Inf. Comput. Sci.* **36** 746
[41] de Fontaine D 1979 *Solid State Phys.* **34** 73
[42] Shang S and Boettger A J 2003 *Acta Mater.* **51** 3597
[43] Pearson W B 1972 *The Crystal Chemistry and Physics of Metals and Alloys* (Chichester: Wiley–Interscience)
[44] Leineweber A, Jacobs H, Hunting F, Luecken H and Kockelmann W 2001 *J. Alloys Compounds* **316** 21

[45] Leineweber A, Jacobs H and Kockelmann W 2004 *J. Alloys Compounds* **368** 229
[46] Lengauer W 2000 *Handbook Ceramic Materials* vol 1, ed R Riedel (Weinheim: Wiley-VCH) pp 202–52
[47] Hahn H and Konrad A 1951 *Z. Anorg. Allg. Chem.* **264** 181
[48] Liu B X, Zhou X and Li H D 1989 *Phys. Status Solidi* a **113** 11
[49] Japel S, Schwager B, Boehler R and Ross M 2005 *Phys. Rev. Lett.* **95** 167801